

Physical Properties of the Spin Hamiltonian on Honeycomb Lattice Samples with Kekulé and Vacuum Polarization Corrections

Ricardo Spagnuolo Martins^{a,b,*}, Elena Konstantinova^c, Humberto Belich^d,
José Abdalla Helayël-Neto^a

^a*Centro Brasileiro de Pesquisas Físicas, 150 Xavier Sigaud Street, Rio de Janeiro, RJ, Brazil*

^b*Instituto Federal de Educação Ciência, e Tecnologia do Triângulo Mineiro, km 167 MG 188 Highway, Paracatu, MG, Brazil*

^c*Instituto Federal de Educação Ciência, e Tecnologia do Sudeste de Minas Gerais, 1283 Bernardo Mascarenhas Street, Juiz de Fora, MG, Brazil*

^d*Universidade Federal do Espírito Santo, 514 Fernando Ferrari Av., Vitória, ES, Brazil*

Abstract

Magnetic and thermodynamical properties of a system of spins in a honeycomb lattice, such as magnetization, magnetic susceptibility and specific heat, in a low-temperature regime are investigated by considering the effects of a Kekulé scalar exchange and QED vacuum polarization corrections to the interparticle potential. The spin lattice calculations are carried out by means of Monte Carlo simulations. We present a number of comparative plots of all the physical quantities we have considered and a detailed analysis is presented to illustrate the main features and the variation profiles of the properties with the applied external magnetic field and temperature.

Keywords: honeycomb lattice, magnetic susceptibility, specific heat, Kekulé, Monte Carlo, vacuum polarization

PACS: 65.80.Ck, 61.48.Gh, 75.30.Cr, 87.10.Rt

1. Introduction

Graphene materials are of a great deal of interest to scientists and engineers from all fields by virtue of their unusual and important properties[14, 16, 15, 26]. The atoms in graphene are arranged in one flat honeycomb (or hexagonal) lattice, so we investigated the effects of some topological deformations in a honeycomb lattice to shed some light on the influence of the topology of the

*Corresponding author

Email addresses: ricardomartins@iftm.edu.br (Ricardo Spagnuolo Martins), elena.konst@ifsudestemg.edu.br (Elena Konstantinova), humberto.belich@ufes.br (Humberto Belich), helayel@cbpf.br (José Abdalla Helayël-Neto)

honeycomb lattice that could possibly be extended to the discussion in graphene samples. In particular, the properties of graphene and graphene-like materials have been deeply inspected from both experimental and theoretical approaches by means of different methods (e.g. see [27, 41, 25, 39, 49] for recent reviews.)

One of the most interesting aspects of graphene, from a theoretical point of view, is the close relation with Quantum Field Theory (QFT)[43, 20, 18, 35]. Such a connection has arisen due to the fact that the dispersion relation is linear near the Dirac points (also called "valleys", and are the points where the energy is zero). This behavior leads to the appearance of low-energy excitations described by a 2-dimensional massless Dirac equation, with a much lower counterpart of the speed of light, v (experimentally $v \sim c/300$). The appearance of quantum anomalies in hexagonal network graphene-type systems is a neat example of this connection [43]. There has been a number of studies addressing fundamental questions of QFT-quantum anomalies [43, 20], and more recently on the relationship between QFT and fractional fermion number [23, 24, 44, 51, 40, 38].

Real graphene surfaces are not perfectly smooth and their physical properties depend on the geometry the deformations, lattice imperfections and also whether the structure has a hollow form, like a sphere, ellipsoid or a tube (i.e. fullerenes and carbon nanotubes) [50, 18, 17].

In the work [2], Chamon discusses the possibility of describing the curvature of a carbon nanotube with a $U(1)$ continuous symmetry, and its implications, related to the Kekulé distortions in the graphene plane. These are natural oscillations of the carbon bond lengths simultaneously stretching and compressing in alternating bonds. His results were supported by [29] at the time. In Ref. [23, 3, 3], this idea is developed in further details. In the work [24], Jackiw and Pi describe how a distortion in a lattice (called Peierls' distortion) can be represented by a coupling of the Dirac field to a massive scalar field, which is a measure of the lattice distortion. They associate this scalar field to the Kekulé texture, as shown in the previous works of Chamon et al. in order to develop a chiral gauge theory of graphene.

From the studies on vortex formation in [23], it comes out that a chiral gauge theory for graphene [24] presents a spinor structure of fermionic zero-mode (fermionic excitations zero energy), which is not modified by the addition of a gauge vector potential chiral coupled with fermions. In fact such coupling promote the idea of magnetic fields fictitious in graphene. This has yielded very fruitful consequences both experimentally and theoretically in the description of elastic deformations and the study of the formation of topological defects with its influences on the electronic properties of graphene [37, 5, 6, 45, 19, 28, 31, 7, 49, 4, 13].

In experimental scenarios, it is possible to observe (by Landau levels measurements) intense pseudomagnetic field (up to 300T) due to tensions in graphene [31]. It is possible to measure, through a microscope of scanning tunneling, Aharonov-Bohm interference due to local deformations in the network [7]. A detailed study of gauge fields in graphene can be found in [49], in a approach of elastic deformations, the emergence of topological defects in a curved environ-

ment is represented by a low-energy Hamiltonian for graphene and some of its effects on electronic properties are discussed [4, 13].

We have explored the idea that these surface imperfections can be described by a scalar massive field and propose that this scalar is a massive propagating degree of freedom that couples electrons and yields an effective interaction, which is spin-dependent and exhibits a screening parameter, ξ , that is the mass of the exchanged boson which we call from now on Kekulé particle.

In this work, we have simulated the physical properties (specific heat, magnetization and magnetic susceptibility) at low temperatures in a honeycomb spin lattice under the influence of the potentials given by the electromagnetic interaction with loop correction and also due to the exchange of the Kekulé boson, in order to account for the non-smoothness of the honeycomb lattice surface. To realize this property, we obtained non-relativistic interaction potentials given by the exchange of a Kekulé particle in a quantum field-theoretic description. The procedure to obtain such potentials from a Feynman diagram was initially stated by Sucher and Feinberg [48, 47, 11, 46]. Essentially, the method consists of examining a scattering via Feynman diagrams and performing a low relativistic approximation on the scattering amplitude. It is shown that this procedure yields the correct interaction potentials previously known, including Coulomb interaction from electron-electron QED scattering, first-order relativistic corrections (known as Breit potential and Gaunt-Moller potential) and Yukawa potential. This method is explored in further details in the works by Dobrescu and Mocioiu [8] and enhanced in the following works [12, 34].

By following this path, we are able to obtain the interaction potentials necessary to simulate the physical properties of graphene that we wish to explore considering the electron-electron scattering mediated by the exchange of a Kekulé boson. We also compared our results with the works of [42, 21], where the specific heat and susceptibility of graphene were analyzed theoretically using renormalization group and gaussian correction methods for low temperatures.

The paper is organized as follows. In Section 2, we describe our method of calculations and state the Hamiltonian used in our simulations. Also, we describe in details all the computational methods, the variables and the units that were used. In Section 3, we present the results of our calculations and discuss their general aspects. Finally, Section 4, we discuss the details and features of our results, present our conclusions and discuss positive and negative aspects of our attempts and the limitations of the simulations we have carried out.

2. Method of calculation

Our model consists of a flat surface square honeycomb lattice of 288 sites. Each site contains a non-itinerant spin, or a vector, that is free to rotate through a fixed point continuously throughout all possible values in a solid angle of 4π but not move among lattices. In other words, we allowed the point of the vector to rotate as if it was inside a sphere, assuming possibly every point in the surface of this sphere. The curvature of the surface is modeled in the interaction

via the Kekulé scalar. In each site, the magnetic moment interact with its neighboring sites by Heisenberg-type and dipole-dipole-type interactions given by the Hamiltonian (1) and also by a vacuum polarization correction potential.

In regard to the issue of quantum interactions among classical agents, we would like to state that we try in this paper to propose and analyze new kind of interaction potentials. These potentials were obtained by an underlying more fundamental physical interactions between fundamental particles. Despite that, these are long range potentials that can reach macroscopic extents and could be present among interaction of classical spins. This is in the heart of the method. The same process of obtaining these kind of potentials described in previous references can also result in classical Coulomb potentials, for example, when considered the quantum interactions of electrons mediated by a photon propagator.

A similar approach was used another recent reference [52] in which they perform an experimental investigation of the contribution of spin interactions of nucleons inside a nucleus of ${}^3\text{He}$, which was theoretically proposed in the same fashion and actually share some of the same references with our work, concerning the process of obtaining these long range interaction potentials.

We have used the Monte Carlo method with the Metropolis algorithm [36, 30, 1]. It was chosen due to its capability to obtain an equilibrium macro-state of a physical system with many coupled degrees of freedom (such as cellular Potts Models and its generalizations, like the Heisenberg model) at a given temperature T . We chose an initial micro-state and performed a very large number of random transformations by a deterministic procedure until we achieve an equilibrium macro-state. The initial micro-state was a parallel array of spins arranged in the sites of a honeycomb lattice. We then randomly changed this configuration and evaluated the change of the overall energy of this new micro-state and compared to the previous configuration. If $\Delta E > 0$, this micro-state replaces the previous one with a probability $e^{-\Delta E/k_b T}$. In a preliminary simulation, we evaluated that the number of steps required to reach the equilibrium state was in the order of $n = 10^4$ for each site in the lattice and we used this number of steps in all of our calculations. The final state corresponded to the stable configuration and was interpreted as the equilibrium macro-state.

Using the method described above, we obtained spin configurations, thermal equilibrium magnetization, magnetic susceptibility and specific heat of the chosen structure. The Hamiltonian for the computed system used was

$$\begin{aligned}
H = & -\vec{B} \cdot \sum_{\langle i,j \rangle} \vec{S}_i - \left(J \sum_{\langle i,j \rangle} \vec{S}_i \cdot \vec{S}_j + \tilde{J} \sum_{\langle i,j \rangle} \frac{e^{-\xi r_{ij}}}{4\pi r_{ij}} \vec{S}_i \cdot \vec{S}_j \right) \\
& - \omega \sum_{i < j} \frac{(\vec{S}_i \cdot \hat{e}_{ij})(\vec{S}_j \cdot \hat{e}_{ij}) - (\vec{S}_i \cdot \vec{S}_j)}{r_{ij}^3} \\
& - \tilde{\omega} \sum_{\langle i,j \rangle} \frac{(3 + 3\xi r_{ij} + \xi^2 r_{ij}^2)(\vec{S}_i \cdot \hat{e}_{ij})(\vec{S}_j \cdot \hat{e}_{ij}) - (1 + \xi r_{ij})(\vec{S}_i \cdot \vec{S}_j)}{4\pi m^2 r_{ij}^3} \\
& + \frac{\alpha}{r_{ij}^2} \sum_{i < j} \left(1 + \frac{\alpha}{4\pi} \frac{e^{-2mr_{ij}}}{(mr_{ij})^{3/2}} \right). \tag{1}
\end{aligned}$$

The first term in the first line, the summation represents the coupling of spins to an external magnetic field B . The terms inside the parenthesis represents the ferromagnetic exchange between the nearest neighbors due to the exchange of a photon and the Kekulé scalar respectively, with coupling constants J and \tilde{J} . The second line is the dipole-dipole interaction due to the electromagnetic interaction with strength ω . The third line stands for the dipole-dipole interaction due to the exchange of the scalar boson with strength $\tilde{\omega}$. The fourth line represent the second order electromagnetic loop correction. The \vec{S}_i 's are the three-dimensional magnetic moments of unit length; \hat{e}_{ij} stands for the unit vectors pointing from the lattice site i to the lattice j and r_{ij} represent the distances between these lattice sites. The quantities ω and $\tilde{\omega}$ may be regarded as the coupling constants for the exchange term and the dipole-dipole interaction respectively. The parameter ξ is the mass of the scalar boson and m is the mass of the electron.

We assume that the external magnetic field is orthogonal to the plane of the structure. The energy and the applied magnetic field are expressed in units of the coupling constant J . The temperature is expressed in the units of J/k_b , where J is the magnitude of the coupling constant and k_b is the Boltzmann constant.

We obtain the magnetic susceptibility χ (in this case along the OZ-axis), by using the Monte Carlo method, according to the expression

$$\chi = \frac{1}{k_b T N} (\langle m_z^2 \rangle - \langle m_z \rangle^2), \tag{2}$$

where N is the number of spins in the system and $\langle m_z \rangle$ is the mean magnetization per spin in the z-direction. the specific heat C is obtained from the energy fluctuations relation

$$C = \frac{1}{k_b T^2 N} (\langle E^2 \rangle - \langle E \rangle^2) \tag{3}$$

where $\langle E \rangle$ is the mean energy per spin. For calculating the specific heat we used $B = 0$.

3. Results

After the general presentation of the Hamiltonian model we have adopted to pursue our investigations, we can from now start off the presentation of the calculations and the corresponding plots for the physical properties we are interested in, namely, the magnetization (Subsection 3.1), the magnetic susceptibility (Subsection 3.2) and the specific heat (Subsection 3.3).

Since there shall be shown many graphs, we have made the option to cast our comments and general discussions of the results we have found in the final Section (Section 4) of our paper.

3.1. Magnetization

We show the results for the calculation of the magnetization in terms of the applied magnetic field for different values of ξ

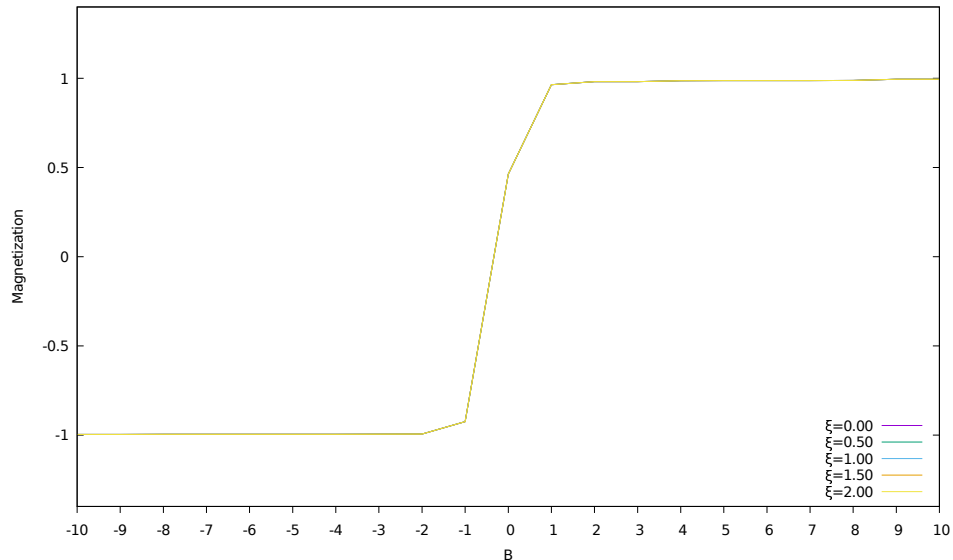


Figure 1: Plots of magnetization versus applied field for all values of ξ for Heisenberg term only. (color online)

In this graph, we calculated the magnetization considering only the Heisenberg interaction. Notice that since there is no exchange of the Kekulé particle, we see only one magnetization curve. There is a full magnetization at about an external field strength of ± 2 , meaning that all spins are aligned. There is a positive magnetization of 0.46 in the absence of the external field and no magnetization at a field value of around -0.3 .

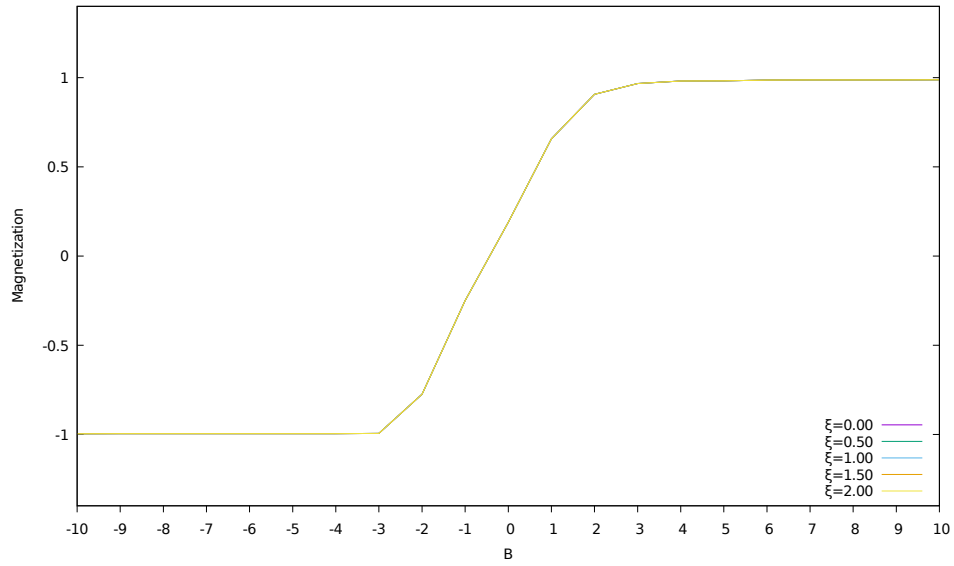


Figure 2: Plots of magnetization versus applied field for all values of ξ , with dipole term included. (color online)

When we include the dipole interaction, we see that the full magnetization occurs at field values of -3 and 4 . In the absence of the external field, the magnetization is 0.19 and there is no magnetization at a field value of -0.5 .

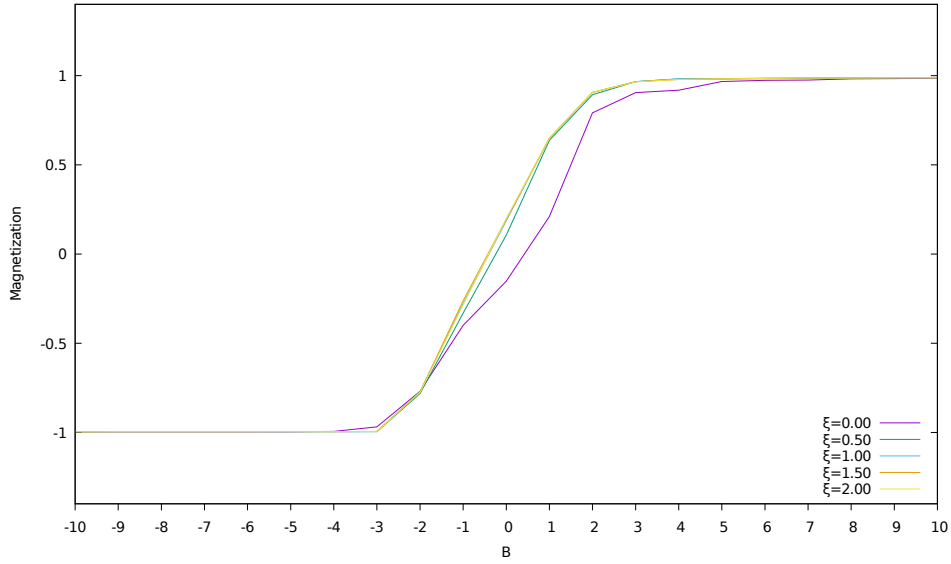


Figure 3: Plots of magnetization versus applied field for all values of ξ , with first Kekulé term included. (color online)

As we include the first Kekulé interaction term, we clearly see a distinct behavior for the magnetization curve of different masses of the Kekulé boson. For higher values of ξ , the magnetization pattern is exactly like 2. We bring the attention to the magnetization curve for $\xi = 0$. It has a magnetization of -0.25 in the absence of the external field and zero magnetization for field values of 0.4 . For the next higher value calculated, $\xi = 0.5$, we see a behavior only slightly different from higher values of ξ .

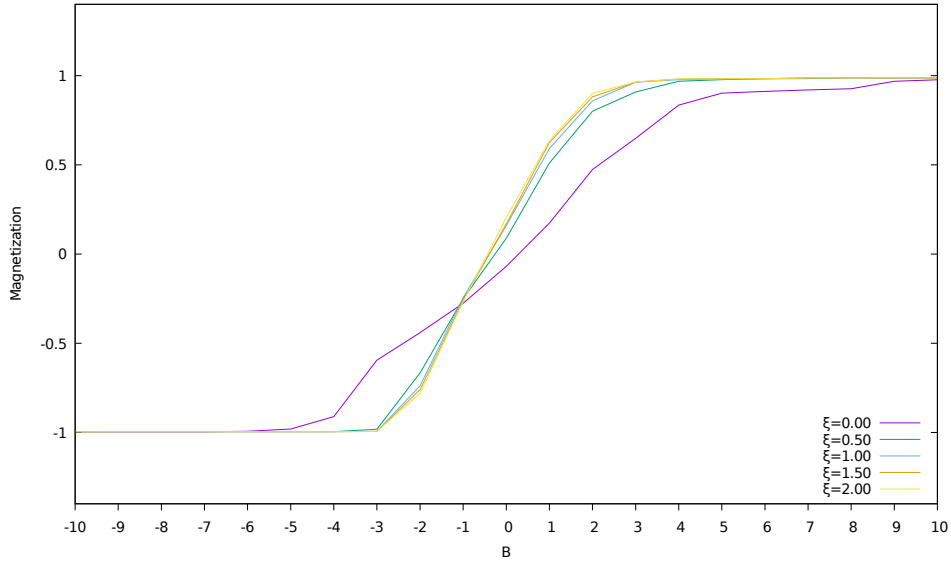


Figure 4: Plots of magnetization versus applied field for all values of ξ , with second Kekulé term included. (color online)

In this calculation, we have all the previous interaction terms and have included the second Kekulé term. The $\xi = 0$ line shows that for a massless Kekulé particle, the material becomes much less responsive to external magnetic fields. We see a clearer differentiation between the higher ξ curves, but they maintain the same behavior as in previous calculations. In order to become fully magnetized for $\xi = 0$, we need to apply a field twice as high as for higher ξ in both orientations.

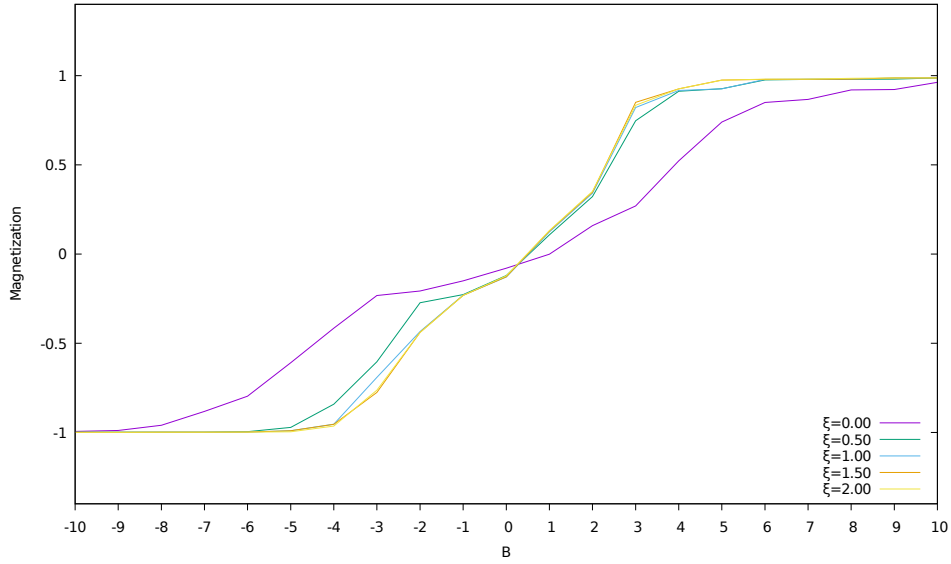


Figure 5: Plots of magnetization versus applied field for all values of ξ , with loop correction included. (color online)

In this calculation, we have included the loop correction term to the previous calculations. The influence of this interaction is clear mainly in the responsiveness to the external magnetic field. All curves need about twice the strength of the external field in order to achieve a full magnetization. Also, all the curves show a negative magnetization in the absence of external fields of -0.12 for $\xi \neq 0$ and -0.08 for $\xi = 0$.

3.2. Susceptibility

Here we present the results of the calculations for the magnetic susceptibility for all values of ξ .

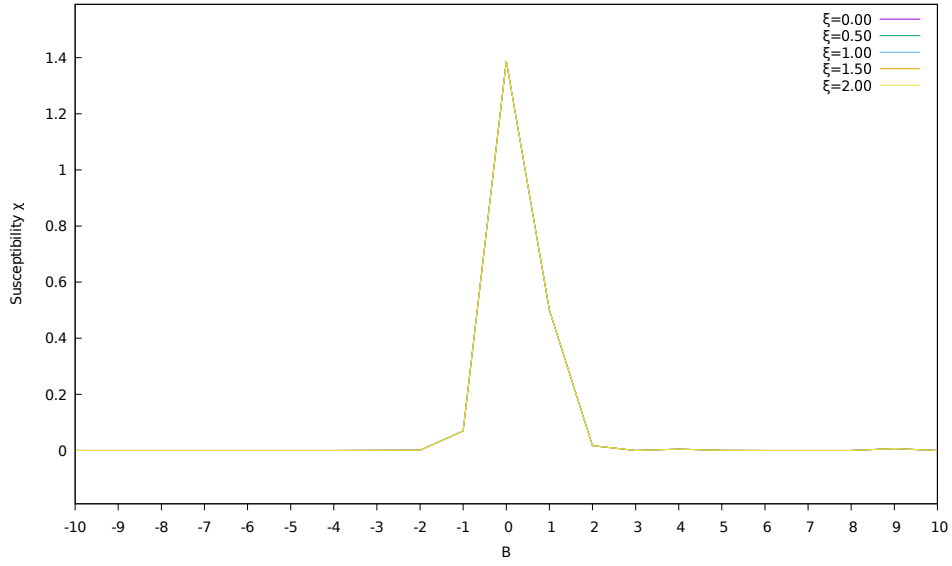


Figure 6: Plots of the magnetic susceptibility versus applied field for all values of ξ , with the Heisenberg interaction. (color online)

We see the highest magnetic susceptibility at $B = 0$, with a small asymmetry for negative and positive external fields, but vanishing quickly for field values of $|B| > 2$.

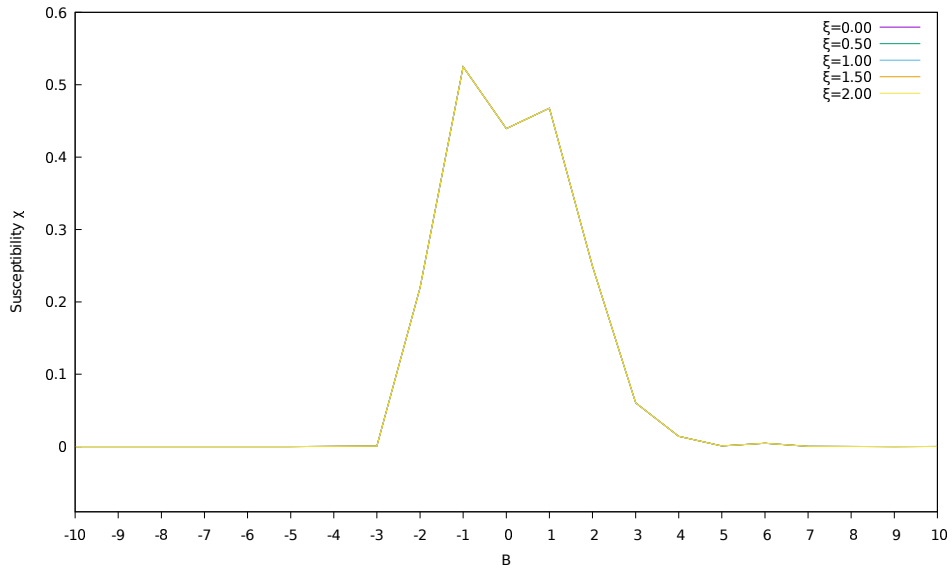


Figure 7: Plots of the magnetic susceptibility versus applied field for all values of ξ , with the dipole interaction included. (color online)

When included the dipole interaction term, the results show now 2 peaks of magnetic susceptibility, being higher for negative fields. Also, notice that the strength of the susceptibility decreases 3 times in comparison to 6.

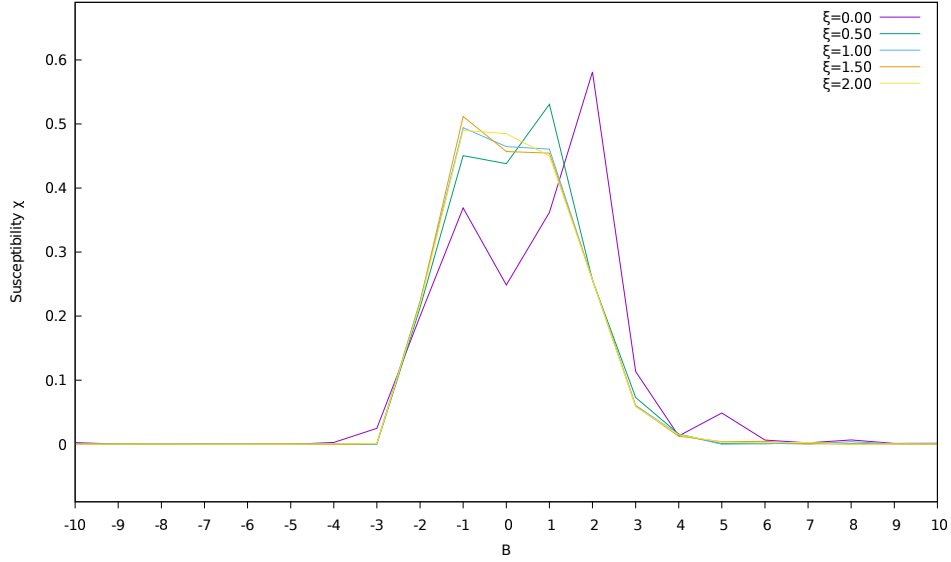


Figure 8: Plots of the magnetic susceptibility versus applied field for all values of ξ , with the first Kekulé term included. (color online)

Here we have included the first Kekulé interaction term to the previous calculations. We clearly see a pattern of asymmetry for the peaks of susceptibility for positive and negative fields, being different for all values of ξ . For the lower values of mass $\xi = 0$ and $\xi = 0.5$, we see that the system responds more strongly to positive fields than negative fields, but that response comes with the cost of applying a stronger positive field than a negative field, e.g., the peak occurs at $B = 2.1$ and $B = -1.0$ for $\xi = 0$. Also, we see a third small peak at $B = 5$ for a massless boson.

For the higher values of mass $\xi = 1.0$ and $\xi = 1.5$, we see the pattern is reversed in relation to the previous lower masses. The lowest peak of magnetic susceptibility is seen for the highest values of ξ , while at $\xi = 2.0$ we can see only one diffuse peak at $B = -1$ that drops sharply for $B > 1.0$.

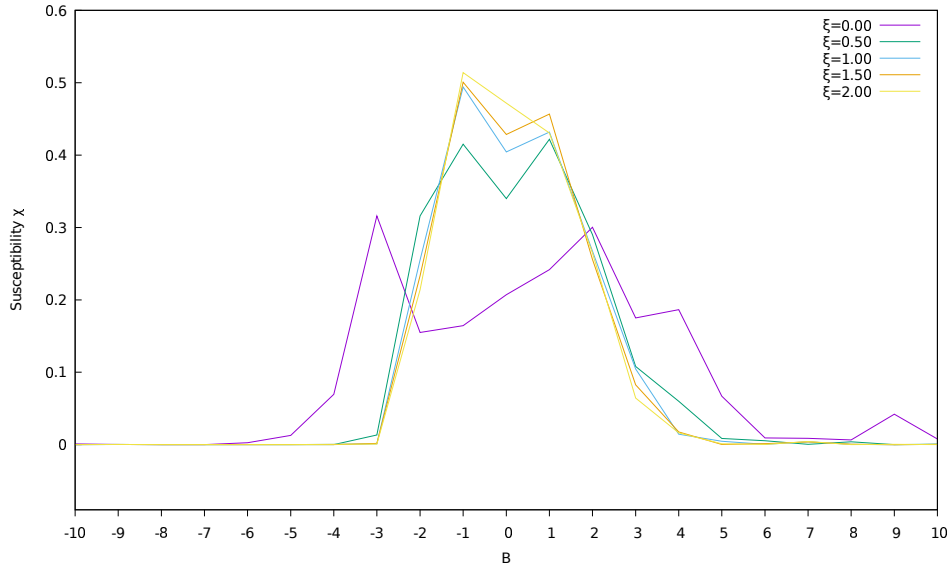


Figure 9: Plots of the magnetic susceptibility versus applied field for all values of ξ , with the second Kekulé term included. (color online)

Here we have include the second Kekulé interaction term to the previous calculations. Now the lowest susceptibilities are seen with the lower values of ξ , a behavior opposite from 8 with a prevalence for negative fields. Again, we see for the highest value of $\xi = 2.0$ what seems to be only one peak, in contrast to 2 peaks for all other values of ξ and what seems to be even 3 peaks for $\xi = 0$.

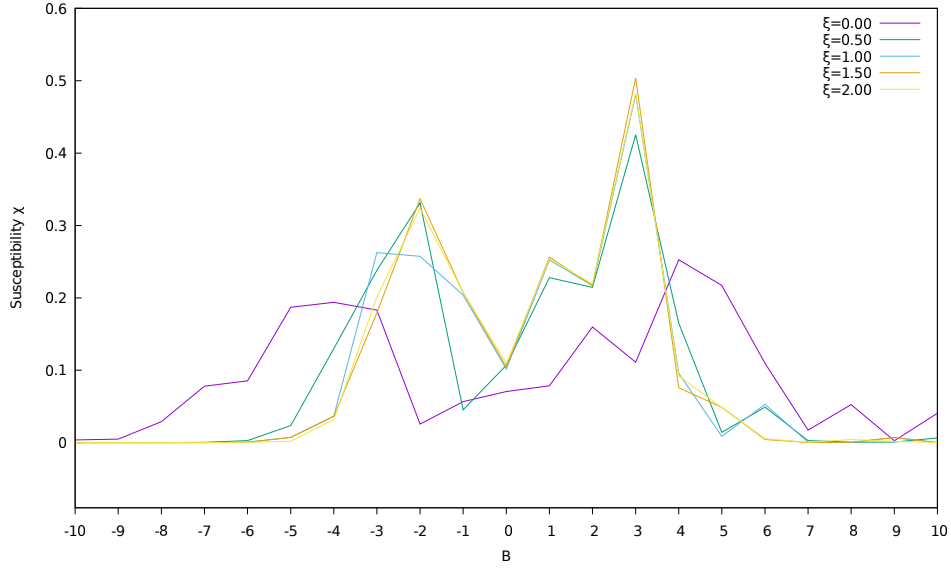


Figure 10: Plots of the magnetic susceptibility versus applied field for all values of ξ , with the loop correction term included. (color online)

In this calculation we have included the loop correction to the previous calculations. Again, we see a shift in the pattern of peaks, now favoring the positive field values, opposite of 9. We bring the attention that with the inclusion of the loop correction, the curve for $\xi = 2.0$ now became very similar to the $\xi = 1.5$ curve, showing 2 distinct peaks.

Also, we point out that in 9, we see for $\xi \neq 0$ that the peaks occur to very low values of the external fields, about ± 1 . In 10, both peaks occur at much higher values of the external field, $B = -2$ and $B = 3$.

3.3. Specific Heat

In this section, we present the results of the calculations for the specific heat for all values of ξ .

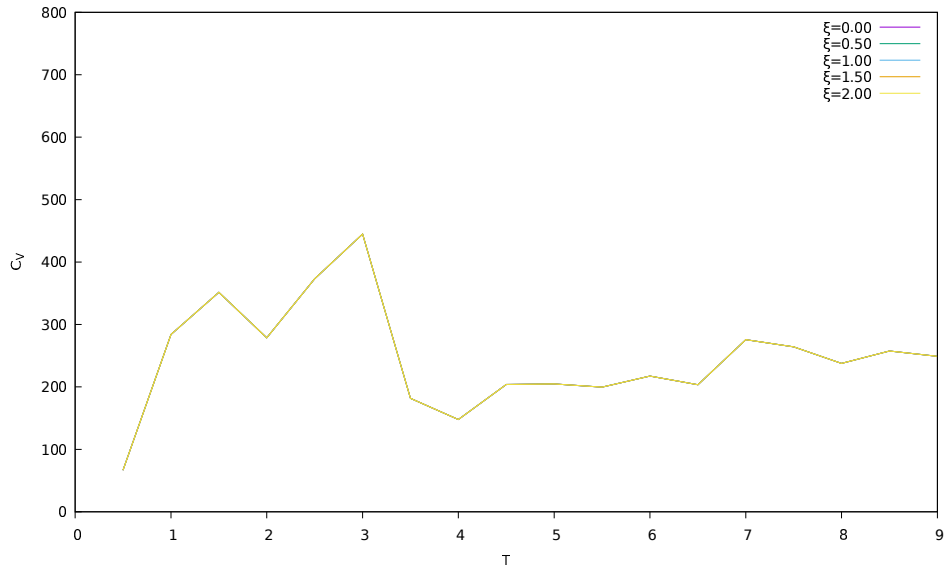


Figure 11: Plots of the specific heat versus temperature for all values of ξ , with only the Heisenberg interaction. (color online)

We see here the results for the specific heat when calculated with only the Heisenberg interaction term. We see a domain of a high specific heat, possibly with two peaks, in the temperature region from 0 to 4. From this temperature on, we see a tendency of increasing specific heat.

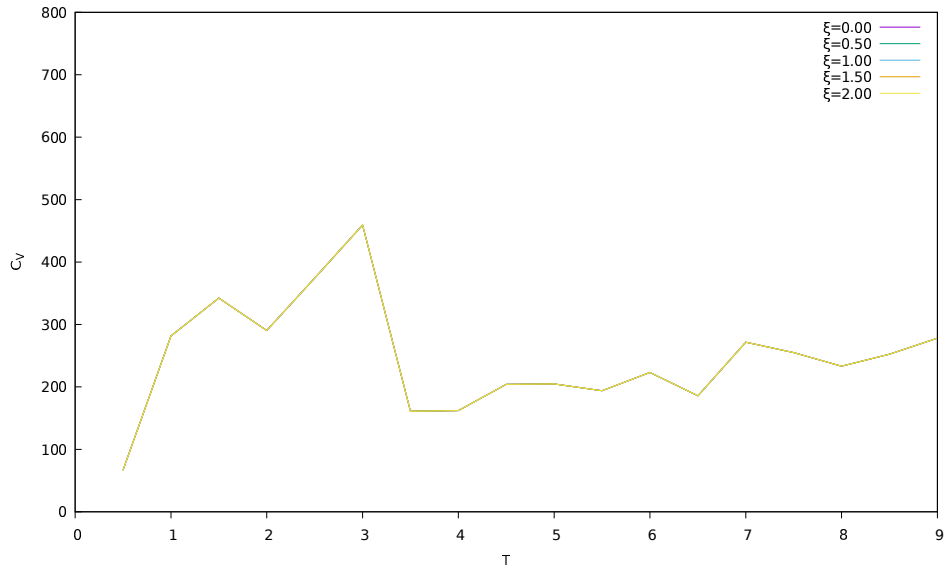


Figure 12: Plots of the specific heat versus temperature for all values of ξ , with the dipole interaction included. (color online)

In figure 12, we have included the dipole interaction term. We see only small changes from 11, barely visible, that can be attributed to the randomization procedure of the Monte Carlo method.

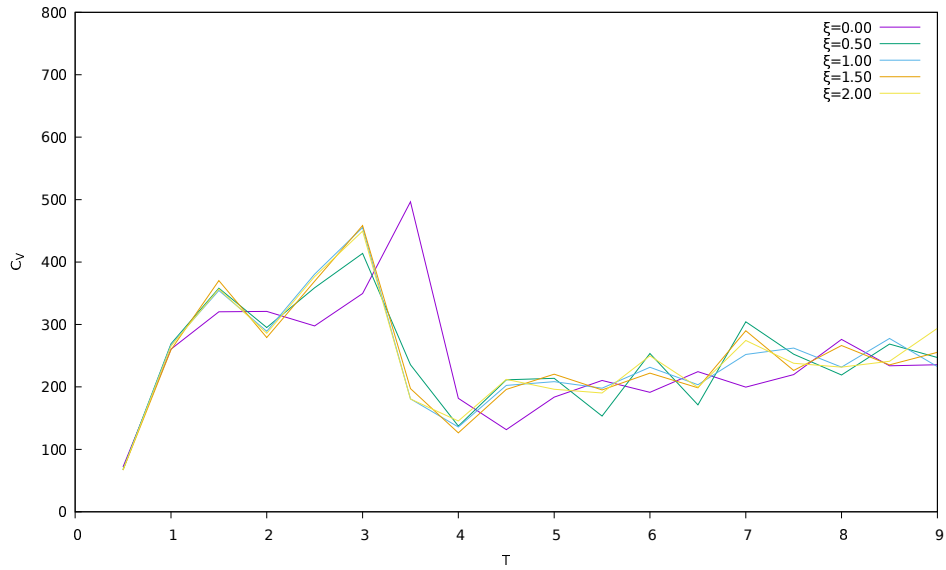


Figure 13: Plots of the specific heat versus temperature for all values of ξ , with the first Kekulé term included. (color online)

Here we have included the first Kekulé term to the previous calculations. Now we can see a difference in behaviour from 11 and 12. The curve for $\xi = 0$ is shifted to the right in relation to the other $\xi \neq 0$ lines. Also, for $\xi = 0$ we have a clear distinctive second peak in the specific heat in relation to the first peak, while for $\xi \neq 0$ we have what looks like two peaks in the region $T = [0; 4]$. For all lines, we have the same increasing specific heat for $T > 4$, with stronger oscillations.

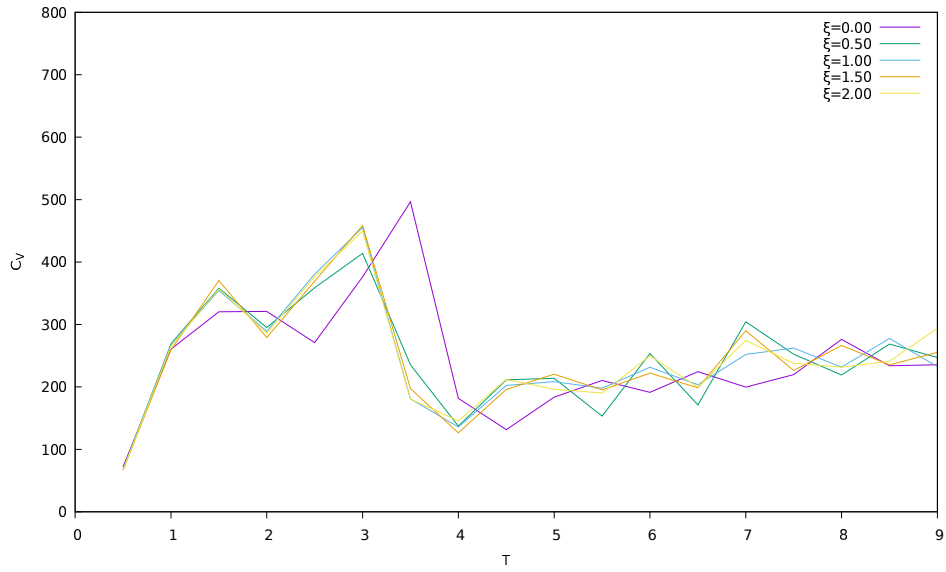


Figure 14: Plots of the specific heat versus temperature for all values of ξ , with the second Kekulé term included. (color online)

Here we have included the second Kekulé term to the previous calculations. We see only small differences from the previous calculation 13 and we assume that they are consistent with fluctuations from the Monte Carlo method.

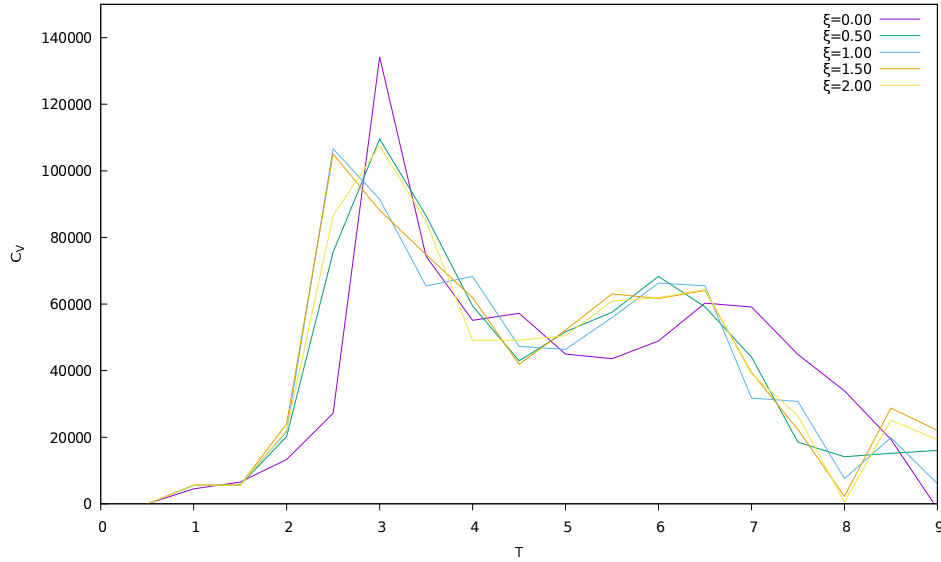


Figure 15: Plots of the specific heat versus temperature for all values of ξ , with the loop correction term included. (color online)

In figure 15, we have include the loop correction term to the previous calculations. This have a great influence on the behavior of the specific heat. We see now only one small, distinctive peak in the region $T = [0; 4]$, arising exponentially from the lower values of T . In the region $T > 4$, we see only an elevation in the line, which then has a decreasing pattern. This contrasts with the increasing pattern in the same region in the previous calculations.

We would like to call the attention to the change in the vertical scale in figure 15. It states that the values of the specific heat are 233 times larger than in previous calculations, indicating a strong influence of the loop correction term to the specific heat.

This is in agreement with [42], which predicts a specific heat for low temperatures proportional to $C_v \propto T^2/|\ln T^2|$ with second order loop corrections.

4. Discussion and final considerations

We have shown that our proposed method of obtaining interaction potentials from quantum field theory and using them to simulate physical systems provide results that can be tested against experiment or compared to other theoretical methods of evaluation. Also, the idea that we explored that the surface curvature of the honeycomb lattice can be modelled by a scalar particle, which we called Kekulé boson, has show to provide differences in the calculated properties that can be looked for in experiments.

In Section 3.1, we have shown that the mass of the Kekulé particle influences the interaction with the external magnetic field. We see in all the calculations

that the higher the mass of the Kekulé boson, the stronger the interaction with the external field is, given all the possible configurations. Since the high mass of the Kekulé boson is related to the curvature of the lattice plane, we conclude that higher curvatures or defects in the planarity of the lattice make the material more subject to the influence of external magnetic fields.

We also see that there is apparently a limit to the value of ξ , or in other words the curvature, can be. We see in figures 3, 4 and 5 that for values of $\xi \geq 1.5$, the difference in the magnetization curve is practically non-existent among those lines, indicating that if we increase the curvature further (i.e. increase the mass), we would have no additional changes to the interaction with the external field.

In relation to the contributions of the individual terms calculated, we conclude that the greatest contribution to the magnetization of the system comes from the the dipole-dipole interaction, aside from the mass ξ . When this term is introduced in the calculations (Fig. 2 and 4 the spins in each lattice interact with each other in such a way that the external field required to promote a full alignment of the spins in the system is 50% greater. As the external field interacts with each site of the lattice, in return each lattice site interact with each other in such a way that the more energetically stable state is the one in which all spins are perpendicular to each other and not parallel. Thus, when this interaction is turned on in our computations, we see an immediate increase in the required external field necessary to align all the spins parallel to each other and also to the external field.

We have shown that in our model, the calculations without the Kekulé particle resulted in a slightly self-magnetic material, with a positive ordering of spins without the influence of an external magnetic field (Fig. 1 and 2). When the Kekulé terms were included in the calculation (Fig. 3 and 4), there was also an ordering of the spin states, but the direction depended on the mass value of the Kekulé particle. For low values of ξ , it showed an overall orientation in the negative direction and for higher values it showed an overall orientation in the positive direction. We could not probe for which value of ξ when the switch from negative to positive occurs, neither for which value there is zero magnetization due to a limitation in our implementation of the algorithm. Our results when included the loop correction term (Fig. 5) showed only negative orientation of spins for all values of ξ , meaning that these second order correction terms may have a strong influence in the ordering of spins in the lattice. Since graphene materials have also honeycomb lattices, we include some references in relation to the highly debated question of intrinsic magnetic properties of graphene (e.g. see the references [27, 32, 10, 9, 22, 33], to which our calculations propose alternative scenarios.

For this type of calculation, our algorithm swept from higher values of the external magnetic field to the lower values in constant steps. We also think that this method for probing the magnetization of the sample could possibly show a characteristic of a hysteresis curve for the magnetization, and this could also explain the asymmetry for positive and negative values of the external field B in for the magnetization.

Our method consider a variety of possible scenarios and possible answers in

each case, but one other limitation from our code implementation is that we rely on experimental input for the parameters used, therefore making it unable to present definitive answers to such questions with high degree of certainty in topics where there is a current debate in literature and experiment. On a positive note, we see that our model is flexible enough to adapt itself in such way that may contemplate the possible scenarios in the debate and give some physical insight in the issue, considering that new interaction terms can be quickly turned on or off in order to account for the physical description inquired.

In the calculations of the magnetic susceptibility, we have shown that each term added to the calculation (magnetic dipole-dipole, Kekulé and loop) changes the susceptibility to an external field, corroborating with the previous results of the magnetization. We see an overall asymmetry in the susceptibility due to positive fields v. negative fields. This is seen both in the range of the existing susceptibility as well as it's intensity. This seems to indicate a preferential direction of application of the magnetic field. This seemingly preferential direction depends directly on the mass of the Kekulé particle, when it is included in the calculations, and also on the magnetic dipole-dipole interactions.

As we have shown in Fig. 6, the strongest susceptibility occurs for very weak fields, both in the positive and negative directions. As we increase the intensity of the applied magnetic field, the susceptibility quickly decreases for negative values of the applied field and about 50% slower for positive values of the applied field before it goes to zero. When the dipole-dipole interactions are turned on in Fig. 7, we still see a slower decrease in the magnetic susceptibility towards positive applied fields. But there is a remarkable difference from only Heisenberg interaction: it increases for weak fields before it decreases for stronger fields. It seems that for weak applied fields, there is a tendency of the spins to respond strongly to the field, as they tend get parallel to each other. This quickly reaches a limit value as the sample increases in the magnetization (more spins get parallel to each other), and to increase further the number of such parallel spins, it must be applied a much stronger magnetic field.

This pattern remains when Kekulé terms are added in 8. When the Kekulé-dipole interaction term was added in 9, this pattern becomes extremely dependent on the value of ξ . For $\xi = 0$, for weak fields we see again a preferential direction towards positive applied fields. The susceptibility increases as the positive field increases, but decreases for negative fields. The spins align themselves faster in the positive direction than in the negative direction. For $|B| = 2$, we see a point of change. For negative values of the field, the spins become aligned faster and for positive values of the field, the rate of alignment of spins reaches a peak value. As we increase the value of ξ , this quickly changes, becoming each time more symmetric around weak fields. For $\xi = 2$, we see another asymmetry occurring. For weak fields, the rate of alignment of the spins increases for negative applied fields, and decreases for positive applied fields, never increasing in the latter and reaching a peak value in the former case. Nevertheless, it still decreases slower for positive applied fields than for negative applied fields. We conclude that the curvature of the lattice plane sheet, or the degree of irregularities, have a strong influence in the magnetic susceptibility of the sample.

When we included also the second order loop correction term in Fig. 10, we still see an asymmetry highly dependent on the value of ξ similar to 9, but as we increase the value of ξ , the magnetic susceptibility pattern tends to maintain the symmetry around weak fields, being virtually the same for $\xi = 1.5$ and $\xi = 2.0$. We still see a preference for positive applied fields for high $|B|$ values, but this is not seen in weak $|B|$ values. This shows that the loop correction effects can be significant when considering this property. In a disclaimer note, we admit to a limitation in our analysis that we can't be sure if we have overestimated or underestimated the loop correction term. The value of the parameter used was obtained via energy optimization considerations and is by no means unique since our calculations were not *ab initio*. The parameters used for the other terms were chosen from a very limited range established using the same considerations used for the loop term, all showing the same characteristics, therefore not posing the same concern for the loop term.

For the calculation of the specific heat, we have shown that the magnetic dipole-dipole interaction does not influence this property, as can be seen in Fig. 12 and Fig. 14. This means that the interaction among spins in the lattice, both via exchange of photons or the Kekulé boson, do not influence in how the lattice stores thermal energy. In other words, the magnetic interactions do not influence the lattice vibrations due to thermal fluctuations.

We saw in Fig. 11 and 13 that the specific heat is slightly dependent on the value of ξ . We see a clear distinction of two regions in the calculations: one with 2 high peaks until a value of approximately $T = 4$ and another where the specific heat steadily increases with some fluctuations for $T > 4$. As we saw in Fig. 13, the value of ξ shifts these patterns sideways. As we increase the values of ξ , the patterns shifts to the left, but we see that this quickly reaches a limit. For $\xi \geq 0.5$, there are only very small changes in the intensities of the peaks but no shifting in their value for T . We also saw that for $\xi > 0$, there is also a higher definition of the first peak in comparison to $\xi = 0$. We did not probe for a higher resolution in the values of ξ to determine the precise value of ξ where this occurs in this work. Although, we see that the influence of the ξ reaches a limit fast in the capacity to store thermal energy, being greater for lower values of ξ and low values of T .

What came as a surprise to us in our calculations was the importance of loop corrections in determining the specific heat of the honeycomb lattice, as seen in Fig. 15. We see an exponential increase in the C_v for low values of T , which was not present in the absence of the loop term. This is consistent with the works of Pei-Song et al. [42]. They calculated the specific heat of graphene due to loop corrections for low temperatures using the renormalization group. In their work, they predicted that the specific heat should have a temperature dependence proportional to $C_v \propto T^2/|\ln T^2|$, which we have reproduced in our model calculations. We have also shown that there is a second and less sharp peak in the specific heat for values of T about two times larger than the first peak. Both peaks have significant higher values than those shown in Fig. 11 and 13. We also saw that the steadily increasing specific heat is absent in Fig. 15, but this could be due to the difference in scale of the previous calculations.

We intend to broaden the range of temperature in future works. We see that the value of ξ has the same peak-shifting property as seen in Fig. 13.

The aforementioned work of Pei-Song et al. [42] also predicted the dependence of the magnetic susceptibility for low values of temperature to be $C_v \propto T/|\ln T^2|$. Our algorithm did not allow for such calculations, and we could not test the authors' prediction, although we have calculated this property and its relation to the applied external magnetic field. We should be able to improve on the algorithm in order to allow for this calculation as well.

The property of the specific heat has shown to have a very low interference from the magnetic dipole-dipole interaction. Both with and without the Kekulé terms, the inclusion of the dipole-dipole type interaction has shown to not change any characteristics of this property. The Kekulé interaction alone was seen to have some influence in the specific heat, mostly considering the calculated values for the mass of the Kekulé scalar. Other than that, it does not alter the main characteristics of this property in relation to the Heisenberg interaction alone. The parameter that mostly affects the specific heat is the loop correction. It increases the value of the property by 233 times, single out one peak value in contrast to two peak values in the $T = [0; 4]$ region and shows a second peak value in the $T > 4$ region with a decreasing value of the property for $T > 7$. The very high peak value obtained in the $T = [0; 4]$ region corroborates with the results obtained by [42] using other theoretical methods of evaluation for the same system.

The authors express their gratitude to the Brazilian Government's Funding Agency, CNPq, for the invaluable financial support.

References

- [1] Kurt Binder and Giovanni Ciccotti. *Monte Carlo and molecular dynamics of condensed matter systems*, volume 49. Compositori, 1996.
- [2] Claudio Chamon. Solitons in carbon nanotubes. *Physica Review B*, 62(4):2806, 2000.
- [3] Claudio Chamon, Chang-Yu Hou, Roman Jackiw, Christopher Mudry, So-Young Pi, and Andreas P Schnyder. Irrational versus rational charge and statistics in two-dimensional quantum systems. *Physical Review Letters*, 100(11):110405, 2008.
- [4] A. Cortijo. PhD thesis, 2007.
- [5] Alberto Cortijo and María AH Vozmediano. Effects of topological defects and local curvature on the electronic properties of planar graphene. *Nuclear Physics B*, 763(3):293–308, feb 2007.
- [6] Fernando de Juan, Alberto Cortijo, and María AH Vozmediano. Charge inhomogeneities due to smooth ripples in graphene sheets. *Physical Review B*, 76(16):165409, oct 2007.

- [7] Fernando de Juan, Alberto Cortijo, María AH Vozmediano, and Andrés Cano. Aharonov-bohm interferences from local deformations in graphene. *Nature Physics*, 7(10):810–815, jul 2011.
- [8] Bogdan A Dobrescu and Irina Mocioiu. Spin-dependent macroscopic forces from new particle exchange. *Journal of High Energy Physics*, 2006(11):005, 2006.
- [9] P. Esquinazi, A. Setzer, R. Höhne, C. Semmelhack, Y. Kopelevich, D. Spemann, T. Butz, B. Kohlstrunk, and M. Lösche. Ferromagnetism in oriented graphite samples. *Physical Review B*, 66(2):024429, jul 2002.
- [10] Pablo Esquinazi and Roland Höhne. Magnetism in carbon structures. *Journal of Magnetism and Magnetic Materials*, 290:20–27, apr 2005.
- [11] Gerald Feinberg, Joseph Sucher, and C-K Au. The dispersion theory of dispersion forces. *Physics Reports*, 180(2):83–157, 1989.
- [12] F. A. Gomes Ferreira, P. C. Malta, L. P. R. Ospedal, and J. A. Helayël-Neto. Topologically massive spin-1 particles and spin-dependent potentials. *The European Physical Journal C*, 75(5):1–10, may 2015.
- [13] T. Fujita, M. B. A. Jalil, S. G. Tan, and S. Murakami. Gauge fields in spintronics. *Journal of Applied Physics*, 110(12):121301, dec 2011.
- [14] A. K. Geim. Graphene: Status and prospects. *Science*, 324:1530–1534, June 2009.
- [15] A. K. Geim and K. S. Novoselov. The rise of graphene. *Nature Materials*, 6:183–191, 2007.
- [16] Andrey K. Geim and Allan H. MacDonald. Graphene: Exploring carbon flatland. *Phys. Today*, 60(8):35-41, Aug 2007.
- [17] T Georgiou, L Britnell, P Blake, RV Gorbachev, A Gholinia, AK Geim, C Casiraghi, and KS Novoselov. Graphene bubbles with controllable curvature. *Applied Physics Letters*, 99(9):093103, 2011.
- [18] J. González, F. Guinea, and M.A.H. Vozmediano. The electronic spectrum of fullerenes from the dirac equation. *Nuclear Physics B*, 406(3):771–794, Oct 1993.
- [19] F. Guinea, B. Horovitz, and P. Le Doussal. Gauge fields, ripples and wrinkles in graphene layers. *Solid State Commun. vol.*, 149:1140–1143, November 2008.
- [20] F. D. M. Haldane. Model for a quantum hall effect without landau levels: Condensed-matter realization of the “parity anomaly”. *Physical Review Letters*, 61(18):20152018, Oct 1988.

- [21] Peisong He. Magnetic susceptibility of graphene by gaussian correction. *International Journal of Modern Physics B*, 25(15):1981–1991, jun 2011.
- [22] Roland Höhne and Pablo Esquinazi. Can carbon be ferromagnetic? *Advanced Materials*, 14(10):753–756, may 2002.
- [23] Chang-Yu Hou, Claudio Chamon, and Christopher Mudry. Electron fractionalization in two-dimensional graphenelike structures. *Physical Review Letters*, 98:186809, 2007.
- [24] R Jackiw and S-Y Pi. Chiral gauge theory for graphene. *Physical Review Letters*, 98(26):266402, 2007.
- [25] M. I. Katsnelson. Graphene: carbon in two dimensions. *Materials Today*, vol., 10:number1–2,pp.20–27, 2007.
- [26] M. I. Katsnelson and K. S. Novoselov. Graphene: new bridge between condensed matter physics and quantum electrodynamics. *Solid State Commun.*, 143,:3–13, 2007.
- [27] Mikhail Iosifovich Katsnelson. *Graphene: carbon in two dimensions*. Cambridge University Press, 2012.
- [28] Eun-Ah Kim and A. H. Castro Neto. Graphene as an electronic membrane. *EPL (Europhysics Letters)*, 84(5):57007, dec 2008.
- [29] Yu. A. Krotov, D.-H. Lee, and Steven G. Louie. Low energy properties of (n, n) carbon nanotubes. *Physical review letters*, 78(22):4245–4248, jun 1997.
- [30] David P Landau and Kurt Binder. *A guide to Monte Carlo simulations in statistical physics*. Cambridge university press, 2014.
- [31] N. Levy, S. A. Burke, K. L. Meaker, M. Panlasigui, A. Zettl, F. Guinea, A. H. C. Neto, and M. F. Crommie. Strain-induced pseudo-magnetic fields greater than 300 Tesla in graphene nanobubbles. *Science*, 329(5991):544–547, jul 2010.
- [32] T. L. Makarova, B. Sundqvist, R. Höhne, P. Esquinazi, Y. Kopelevich, P. Scharff, V. Davydov, L. S. Kashevarova, and A. V. Rakhmanina. Retraction: Magnetic carbon. *Nature*, 440(7084):707–707, mar 2006.
- [33] Tatiana L Makarova, Bertil Sundqvist, Roland Höhne, Pablo Esquinazi, Yakov Kopelevich, Peter Scharff, Valerii A Davydov, Ludmila S Kashevarova, and Aleksandra V Rakhmanina. Magnetic carbon. *Nature*, 413(6857):716–718, 2001.
- [34] P. C. Malta, L. P. R. Ospedal, K. Veiga, and J. A. Helayël-Neto. Comparative aspects of spin-dependent interaction potentials for spin-1/2 and spin-1 matter fields. *Advances in High Energy Physics*, 2016:1–13, 2015.

- [35] EC Marino, Leandro O Nascimento, Van Sergio Alves, and C Morais Smith. Interaction induced quantum valley hall effect in graphene. *Physical Review X*, 5(1):011040, mar 2015.
- [36] Nicholas Metropolis, Arianna W. Rosenbluth, Marshall N. Rosenbluth, Augusta H. Teller, and Edward Teller. Equation of state calculations by fast computing machines. *The Journal of Chemical Physics*, 21(6):1087, 1953.
- [37] Jannik C Meyer, Andre K Geim, Mikhail I Katsnelson, Konstantin S Novoselov, Tim J Booth, and Siegmur Roth. The structure of suspended graphene sheets. *Nature*, 446(7131):60–63, mar 2007.
- [38] Antti Juhani Niemi and Gordon W Semenoff. Fermion number fractionization in quantum field theory. *Physics Reports*, 135(3):99–193, apr 1986.
- [39] K. S. Novoselov, A. K. Geim, S. V. Morozov, D. Jiang, M. I. Katsnelson, I. V. Grigorieva, S. V. Dubonos, and A. A. Firsov. Two-dimensional gas of massless dirac fermions in graphene. *Nature*, 438:197–200, 2005.
- [40] Angel E Obispo and Marcelo Hott. Fractional fermion charges induced by axial-vector and vector gauge potentials and parity anomaly in planar graphenelike structures. *Physical Review B*, 89(16):165405, apr 2014.
- [41] Swapan K Pati, Toshiaki Enoki, and Chintamani Nagesa Ramachandra Rao. *Graphene and its fascinating attributes*. World Scientific, 2011.
- [42] He Pei-Song, Oh Sung-Jin, Chen Yu, and Tian Guang-Shan. Specific heat and magnetic susceptibility of graphene: A renormalization group study. *Communications in Theoretical Physics*, 54(5):897–907, nov 2010.
- [43] Gordon Semenoff. Condensed-matter simulation of a three-dimensional anomaly. *Physical Review Letters*, 53(26):2449–2452, Dec 1984.
- [44] Babak Seradjeh and Marcel Franz. Fractional statistics of topological defects in graphene and related structures. *Physical review letters*, 101(14):146401, sep 2008.
- [45] Yu.A. Sitenko and N.D. Vlasii. Electronic properties of graphene with a topological defect. *Nuclear Physics B*, 787(3):241–259, dec 2007.
- [46] J. Sucher. Potentials from field theory: Non-uniqueness, gauge dependence and all that. In *AIP Conference Proceedings*, volume 189, page 337. AIP Publishing, 1989.
- [47] J. Sucher. What is the force between electrons? pages 433–443, 2007.
- [48] J. Sucher. The concept of potential in quantum field theory. 2008.
- [49] M.A.H. Vozmediano, M.I. Katsnelson, and F. Guinea. Gauge fields in graphene. *Physics Reports*, 496(4-5):109–148, Nov 2010.

- [50] Mara A H Vozmediano, Fernando de Juan, and Alberto Cortijo. Gauge fields and curvature in graphene. In *Journal of Physics: Conference Series*, volume 129, page 012001. IOP Publishing, oct 2008.
- [51] C Weeks and M Franz. Interaction-driven instabilities of a dirac semimetal. *Physical Review B*, 81(8):085105, feb 2010.
- [52] W. Zheng, H. Gao, B. Lalremruata, Y. Zhang, G. Laskaris, W. M. Snow, and C. B. Fu. Search for pin-dependent short-range force between nucleons using optically polarized ^3He gas. *Physical Review D*, volume 85, page 031505, 2012.